Title: Microbiota-derived secondary bile acids promote STING activation and antitumor activity

Authors: Xinglin Yang[1,4*†], Xing Zhang[1†], Weichao Li[2], Anant Gharpure[3], Althea Hansel-Harris[3], Andreas F. Tillack[3], Chongyang Wu[1], Yan-Zhu Hsieh[1], Ariana Sulpizio[2], Stanislav Dikiy[1], Xiaohui Zhao[1], Stefano Forli[3], Luke L. Lairson[2], Andrew Ward[3], Christopher G. Parker[2], Howard C. Hang[1,2*]

Affiliations:

[1] Department of Immunology and Microbiology, Scripps Research

[2] Department of Chemistry, Scripps Research

[3] Department of Integrative Structural and Computational Biology, Scripps Research

[4] State Key Laboratory of Natural and Biomimetic Drugs, School of Pharmaceutical Sciences, Chemical Biology Center, Peking University

[†]These authors contributed equally to this work

*Corresponding authors. xlyang@bjmu.edu.cn (X. Y.); hhang@scripps.edu (H. C. H.).

Abstract: Microbiota metabolism generates diverse bile acids that are associated with health and disease, but the molecular targets and mechanisms of action for these metabolites have not been fully elucidated. Using bile acid photoaffinity probes and chemoproteomics, we found many protein targets of microbiota-derived secondary bile acids in mammalian cells. Of note, we discovered deoxycholic acid (DCA) binds the transmembrane domain of stimulator of interferon genes (STING), promotes its oligomerization and agonist stimulation of type I interferon signaling *ex vivo* and antitumor immunity *in vivo*. Moreover, oral administration of DCA-producing microbiota species enhanced STING agonist antitumor immunity *in vivo*. This reverse chemical microbiology approach revealed an unpredicted mechanism of action for DCA on STING regulation and suggests specific secondary bile acids and their associated microbiota species may impact the efficacy of STING-targeted therapeutics.

One-Sentence Summary: Microbiota-derived DCA binds to transmembrane domain of STING and promotes its activation of immune signaling and antitumor immunity.

Main Text:

Bile acids are sterol metabolites that are associated with diverse phenotypes in health, disease and therapy responses(*1*), but their specific mechanisms of action are still enigmatic. Biosynthesis of bile acids starts with oxidation and hydroxylation of cholesterol in the liver followed by conjugation with glycine or taurine to generate primary bile acids(*1*). Export of primary bile acids into the intestine facilitates cholesterol turnover and disposal as well as aids in digestion. In the gut, primary bile acids are deconjugated, oxidized and epimerized by specific microbiota species to generate a variety of secondary bile acids(*2-5*) (**Fig. 1A**). These structurally diverse microbiota-derived bile acids have been implicated in variety physiological processes, ranging from direct antibacterial activity(*6, 7*) to modulation of host metabolism(*8, 9*), immunity(*10*), viral infection(*11, 12*), vaccine responses(*13*), aging(*7, 14*) and tumor progression (*15-18*). However, only a few molecular targets and mechanisms of actions for specific bile acids have been described(*9*). Of note, bile acids were discovered as endogenous ligands for farnesoid X receptor (FXR), which regulates the expression of target genes involved in hepatic bile acid synthesis, secretion and intestinal re-absorption(*19, 20*). In addition, the G-protein coupled receptor TGR5 has been reported to sense bile acids and regulate intestinal homeostasis and inflammation(*10, 21*). Moreover, secondary bile acids have been reported to bind and regulate the activity of specific nuclear hormone receptors like RORγt and NR4A1 in T cells to control their differentiation and activation(*22-26*). Secondary bile acids have also been shown to phenocopy anti-aging effects of calorie restriction by binding TUB-like protein 3(*14, 27*). Metabolomic studies indicate hundreds of additional conjugated and unconjugated bile acids can be found in different mammalian tissues(*4, 9*), which necessitates further mechanistic and functional studies.

To address the mechanisms of actions for different bile acids, we and others have generated photoaffinity probes to identify and validate their protein targets in bacteria(*28-31*) and mammalian cells(*27, 32*) (**Fig. S1A**). In this study, we focused on deoxycholic acid (DCA) (**Fig. 1A**), as this microbiota-derived secondary bile acid has been reported to modulate host immunity(*11, 13*) and also been developed a therapeutic to reduce submental fat(*33*), but the protein targets of DCA and its mechanisms of action were largely unexplored. DCA is a secondary bile acid generated by the gut microbiota dehydroxylation of cholic acid (CA) (**Fig. 1A**). The removal of a hydroxyl group at the C7 of the sterol significantly alters the physicochemical properties of the bile acid, potentially conferring unique membrane penetrating and protein binding capabilities of DCA. Using different photoaffinity probes for DCA and CA (**Fig. 1B, Fig. S1A**), our quantitative comparative chemoproteomic analysis of human monocyte (THP-1) cell line revealed many candidate DCA-selective protein targets (**Fig. 1C, D**), including sterol metabolic enzymes, membrane proteins, nuclear receptors and immunity-associated proteins (**Fig. S1B, Tables S1-3, supplementary Data S1**). Notably, STING (TMEM173) was one of the DCA-selective protein targets compared to CA and can be competed off by excess of DCA (**Fig. 1C, D, Fig. S1B**). Western blot analysis of photoaffinity probe-enriched proteins showed that STING was crosslinked by the DCA probes, but not the CA probe, which was significantly reduced when THP-1 cells were co-incubated DCA (**Fig. 1E**). DCA also reduced photoaffinity probe crosslinking of FXR and STING endogenously expressed in HT-29 cells (**Fig. S1C**) and human STING overexpressed in HEK293T cells (**Fig. S1D**). These results suggest that DCA may directly bind STING in mammalian cells.

STING is a critical immune sensor activated by cyclic dinucleotides (CDNs), which can be synthesized by cyclic GMP-AMP synthase (cGAS) in response to endogenous cytosolic DNA fragments or from pathogens during infection(*34, 35*). Upon binding CDNs, STING that localized to the endoplasmic reticulum (ER), oligomerizes, translocates to endolysosomes and forms a complex with TANK-binding kinase 1 (TBK1). TBK1 then phosphorylates itself, STING and transcription factors such as interferon regulatory factor 3 (IRF3), which activates IRF3 to induce the production of type I interferons (IFNs) and other cytokines to promote immune responses against infections and tumors(*36, 37*). In addition, TBK1 recruitment to STING also activates NF-κB signaling.(*38*) Based on these properties, synthetic agonists for STING have been developed as therapeutic leads to treat infections(*39, 40*) and cancer(*41, 42*). Of note, compounds that mimic CDNs such as diABZI(*43*), SR-717(*44*) and MSA-2(*45*) (**Fig. S2A**) have been shown to target the CDN-binding domain of STING and potently induce the expression of type I IFN responses. Furthermore, compounds such as C53(*46*) and NVS-STG2(*47*) that bind the transmembrane domain of STING also promote its oligomerization and immune activation (**Fig. S2B**). We therefore investigated if DCA alone or in combination with STING agonists modulated type I IFN responses. Using an IFN-β luciferase reporter assay, we found that DCA but not CA enhanced the activity of CDNs (cGAMP and c-di-AMP) and synthetic STING agonists such as diABZI (**Fig. 2A, Fig. S2E**). DCA alone did not significantly activate STING at concentrations up to 200 μM, but enhanced the activity of diABZI in a dose-dependent manner by measuring STING phosphorylation in THP-1 cells (**Fig. S2C,D**). To further investigate the STING activation, we measured the expression of IFN-β, CXCL10, and IL-6 in both THP-1 and RAW264.7 (murine macrophage cell line) using RT-qPCR (**Fig. 2B**). Co-treatment with DCA and diABZI induced significantly higher levels of these cytokines compared to either treatment alone (**Fig. 2B**). Treatment of THP-1 cells with DCA and diABZI increased the phosphorylation of STING, TBK1, and IRF3 compared to either compound alone, which was also abrogated in STING knockout (KO) cells (**Fig. 2C**).

To further explore STING activation, we transfected differentiated THP-1 cells with high molecular weight DNA (HT-DNA), which activates cGAS to produce endogenous cGAMP and observed DCA enhancement of HT-DNA induced STING activation (**Fig. S3A**). DCA also enhanced the activity of other synthetic STING agonists (SR-717, MSA-2 and DMXAA) in HEK293T cells expressing human STING and an IFN-β reporter (**Fig. S3B**) as well as other STING variants, including murine STING, STING-HAQ (R71H, G230A and R293Q), and STING-232H (R232H)(*48*) (**Fig. S3C**). DCA enhancement of STING activation was also observed with CDNs (**Fig. 2D,E**) and diABZI in primary human peripheral blood mononuclear cells (PBMCs) (**Fig. 2F,G, Fig S2F**) as well as differentiated THP-1 (**Fig. S3D**) and HT-29 cells (**Fig. S3E**). We also observed more STING puncta formation (**Fig. S4A**) and oligomerization (**Fig. S4B**) in cells that were co-treated with diABZI and DCA, but not CA. To assess the specificity of BAs on STING activation, we compared the effects of different conjugated and free bile acids. DCA consistently exhibited the most potent activity among all tested BAs (**Fig. S5A**). Structural modifications at the 3-hydroxyl position, such as isomerization or oxidation, significantly reduced DCA enhancement of STING activation (**Fig. S5A**). Interestingly, alloLCA, but not LCA or isoLCA, showed comparable levels of DCA enhanced STING activation (**Fig. S5A**). Collectively, these results demonstrate DCA, amongst the BAs tested, most effectively enhances STING activation in a variety of different cell types *ex vivo*.

To investigate the binding site of DCA on STING, we conducted competitive ligand photoaffinity crosslinking studies in cells and structural studies *in vitro*. Notably, NVS-STG2 a synthetic molecule reported to target the STING dimer-dimer interface reduced DCA probe photocrosslinking with STING in cells (**Fig. 3A,B**). In contrast, diABZI which binds the CDN-binding domain failed to affect the DCA probe-STING photocrosslinking, even with 10-fold excess (**Fig. S5C**). Interestingly, pre-treatment of THP-1 cells with diABZI enhanced the interaction between the DCA probe and STING (**Fig. 3C,D**). This enhanced interaction was suppressed by BB-Cl (**Fig. 3C,D**)(*49*), an inhibitor of STING activation (**Fig. S5B**). To elucidate the DCA-STING binding site, we employed single-particle cryo-electron microscopy (cryo-EM). We included STING agonists cGAMP and C53 to capture the ligand-activated protein state and stabilize potential oligomers, similar to previous studies with NVS-STG2(*50*). From these studies, we obtained a 2.9 Å resolution map of a STING tetramer complexed with ligands (cGAMP, C53 and DCA) (**Fig. S6**). Notably, we observed additional molecular density between the transmembrane domains of STING dimers (**Fig. 3E**), which was absent in the STING-cGAMP-C53 structure(*46*), suggesting this region as a potential binding site for secondary bile acids like DCA.

To model DCA into the putative binding site in STING, we used a custom Monte-Carlo docking engine. Affinity grid maps were calculated with the AutoDock4.2 force field and modified using our CryoXKit(*51*) software to include guidance from the C2-symmetric cryo-EM density. The resulting docked model is shown in **Fig. 3F**, where we have modeled one bile acid molecule into one half of the C2 map. The carboxylate of DCA forms strong charge-charge interactions with R94 of both the A (red) and C (blue) STING monomers, vertically orienting the ligand parallel to the surrounding helices. The rest of the molecule forms interactions mostly with the A and B (yellow) monomers. This single, static binding pose only explains a limited portion of the observed ligand density. Therefore, we generated a Boltzmann-weighted map of all poses sampled during the docking simulation, to better represent the full volume sampled during the run and allow for more direct comparison to the cryoEM density. Notably, this map also includes the sampled positions of oxygens and polar hydrogens that may be poorly resolved in the corresponding cryoEM density. The docking Boltzmann map (outer purple surface in **Fig. 3G**) shows that the docking does largely sample all the cryoEM density volumes assigned to the ligand, including those not explained by the single predicted binding pose. The only exception here is a single lobe of cryoEM density only appearing in the C2 map (**Fig. 3G** right) but not the asymmetric C1 map, suggesting DCA binding in the pocket is asymmetric. These results suggest that DCA may bind at the STING transmembrane dimer-dimer interface to enhance oligomerization and promote agonist-induced activation.

To validate the proposed binding site, we generated STING transmembrane mutants and assessed their response to diABZI and DCA. Several mutants, including R94F, R95F, and L136E, exhibited reduced sensitivity to DCA-induced enhancement of STING activation (**Fig. 3H, I, J**). In contrast, other mutants, such as L136A, L136K, and L136R, showed increased sensitivity to DCA activation (**Fig. 3H**). These mutagenesis data support the model that DCA binds directly to the STING transmembrane domain near the dimer-dimer interface. Molecular docking of other bile acids (**Fig. S5D**) shows the inactive sterols (CA, iso-DCA, UDCA and iso-LCA) do not make ideal contacts with STING transmembrane dimer-dimer interface compared to other active secondary bile acids such as alloLCA (**Fig. S5A**), which adopts similar conformation to DCA (**Fig. 3F**). Together, these

findings indicate that secondary bile acids such as DCA binds to a large pocket at the STING transmembrane dimer-dimer interface to enhance its ligand-induced oligomerization and activation of downstream signaling.

To test whether bile acids promote STING activation *in vivo*, we evaluated the activity of CA and DCA in mouse models. Notably, intraperitoneal (IP) injection of diABZI (1 mg/kg) with bile acids showed DCA, but not CA, synergizes with STING activation and enhanced type I interferon (IFN-I) activation, as shown by IFN-β levels in the serum (**Fig. S7A, B**). In addition, DCA synergized with CDN STING agonist such as c-di-AMP to enhance serum levels of IFN-β (**Fig. S7C**). As STING activation has been shown to promote antitumor immunity(*41, 42*), we also evaluated the bile acids with diABZI in tumor models. For these studies, we employed intratumoral (IT) injection of the compounds (**Fig. 4A**) in the B16F10 melanoma tumor model(*52*) and utilized a lower dose of diABZI to observe potential synergistic effects of the bile acids (**Fig. S8A**). IT injection of DCA (2.5 mg/kg) combined with a low dose of diABZI (50 μg/kg) significantly reduced tumor size, whereas neither treatment alone showed an effect (**Fig. 4B**). Notably, this effect was DCA-specific, as CA together with diABZI showed no antitumor activity against B16F10 melanoma tumors (**Fig. 4C, S8B**). We found that DCA also promoted diABZI-induced STING antitumor activity with less immunogenic Panc02 pancreatic tumors(*53*)(**Fig. S8C**), whereas DCA did not have a significant effect on highly immunogenic MC38 colonic tumors(*41*) (**Fig. S8D**). To investigate the antitumor immune response, we analyzed the tumor-infiltrating lymphocytes (TILs), tumor-draining lymph nodes (tdLN) and spleen B16F10 melanoma tumor model by flow cytometry (**Fig. S9A**). In tdLN and spleen, the STING activation marker, Sca-1, was significantly induced following diABZI treatment, both with and without DCA, in tdLN and spleen (**Fig. S10A**). In TILs, we found no differences in the absolute number of $CD45^+$ leukocytes or $CD3^+$ lymphocytes (**Fig. S10B**). However, in TILs, the combination treatment significantly increased the levels of Sca-1^+ $CD8^+$ T cells, along with other $CD8^+$ T cells activation markers, including granzyme B, Ki67, CD69 and PD-1 (**Fig. 4D**). The $NK1.1^+$ cells and granzyme B^+ $NK1.1^+$ cells were also increased in TILs with the combination treatment group (**Fig. S10C, D**). These results show DCA enhancement of STING activation in TILs is sufficient to promote antitumor immunity *in vivo*.

Our discovery that DCA modulates STING activation suggests that specific microbiota species capable of producing secondary bile acids may regulate this immune signaling pathway *in vivo*. Notably, recent metabolomic and genetic studies revealed that *Clostridium scindens*, but not *Clostridium sporogenes*, expresses the *bai* operon, which is responsible for producing secondary bile acids in the gut(*6, 54*). To investigate whether DCA-producing microbiota modulates STING activation *in vivo*, we colonized antibiotic-treated mice with *C. scindens* (DCA-producing bacteria, ATCC 35704) or *C. sporogenes* (control, ATCC 15579) and evaluated their effects on IT-injection of diABZI STING agonist in B16F10 tumor model (**Fig. 4E**). We found that colonization with *C. scindens*, but not *C. sporogenes*, synergized with diABZI to reduce B16F10 tumor size (**Fig. 4F**). Importantly, *C. scindens* colonization in the absence of diABZI, did not exhibit antitumor activity (**Fig. S11**). We also evaluated conventional specific pathogen-free (SPF) mice with intact microbiota and observed *C. scindens* similarly synergized with diABZI to enhance antitumor activity (**Fig. 4G**) and increase the numbers of granzyme B^+ CD8 T cells in TILs (**Fig. 4H**). Our findings demonstrate that DCA-producing microbiota species such as *C. scindens* can also synergize with STING agonists to enhance antitumor immunity *in vivo*.

The diversity of microbiota species and metabolites represents a major challenge for functional studies in health, disease and therapy response. Using a reverse chemical microbiology approach(*55*), our proteomic analysis of microbiota-derived bile acid protein targets revealed a previously unpredicted functional interaction between DCA and the innate immune sensor STING. Through cell signaling, cellular photocrosslinking and cryo-EM studies, we demonstrated that DCA, but not its primary bile acid precursor CA, binds to the transmembrane dimer-dimer interface of STING and promotes its oligomerization and stimulation of immune signaling. Furthermore, our studies show DCA and DCA-producing microbiota species can promote the antitumor activity of STING agonists *in vivo*. Of note, secondary bile acids have been shown to suppress antitumor immunity and promote cancer progression(*15-18*). However, our studies establish an unpredicted functional link between microbiota-derived secondary bile acids such as DCA and STING signaling, which suggest that the microbiota and bile acid composition of patients may impact the efficacy of STING-targeted therapies for antitumor immunity(*42*). Furthermore, as highly potent synthetic STING agonists exhibit significant on-target and cell type-dependent toxicities(*42*), the synergistic activity of DCA and DCA-producing microbiota species we observe with lower doses of STING agonist may be leveraged to improve the efficacy of these immunotherapies for cancer and other diseases(*7, 11, 12, 39, 40, 56, 57*).

References and Notes

1. A. F. Hofmann, L. R. Hagey, Key discoveries in bile acid chemistry and biology and their clinical applications: history of the last eight decades. *J Lipid Res* **55**, 1553-1595 (2014).
2. R. A. Quinn *et al.*, Global chemical effects of the microbiome include new bile-acid conjugations. *Nature* **579**, 123-129 (2020).
3. E. C. Gentry *et al.*, Reverse metabolomics for the discovery of chemical structures from humans. *Nature* **626**, 419-426 (2023).
4. I. Mohanty *et al.*, The underappreciated diversity of bile acid modifications. *Cell* **187**, 1801-1818 e1820 (2024).
5. T. H. Won *et al.*, Host metabolism balances microbial regulation of bile acid signalling. *Nature* **638**, 216-224 (2025).
6. C. G. Buffie *et al.*, Precision microbiome reconstitution restores bile acid mediated resistance to Clostridium difficile. *Nature* **517**, 205-208 (2015).
7. Y. Sato *et al.*, Novel bile acid biosynthetic pathways are enriched in the microbiome of centenarians. *Nature* **599**, 458-464 (2021).
8. Q. Nie *et al.*, Gut symbionts alleviate MASH through a secondary bile acid biosynthetic pathway. *Cell* **187**, 2717-2734.e2733 (2024).
9. I. Mohanty *et al.*, The changing metabolic landscape of bile acids – keys to metabolism and immune regulation. *Nature Reviews Gastroenterology & Hepatology* **21**, 493-516 (2024).
10. M. H. Lee *et al.*, How bile acids and the microbiota interact to shape host immunity. *Nature Reviews Immunology* **24**, 798-809 (2024).
11. E. S. Winkler *et al.*, The Intestinal Microbiome Restricts Alphavirus Infection and Dissemination through a Bile Acid-Type I IFN Signaling Axis. *Cell* **182**, 901-918 e918 (2020).

12. M.-M. Hu *et al.*, Virus-induced accumulation of intracellular bile acids activates the TGR5-β-arrestin-SRC axis to enable innate antiviral immunity. *Cell Research* **29**, 193-205 (2019).
13. T. Hagan *et al.*, Antibiotics-Driven Gut Microbiome Perturbation Alters Immunity to Vaccines in Humans. *Cell* **178**, 1313-1328.e1313 (2019).
14. Q. Qu *et al.*, Lithocholic acid phenocopies anti-ageing effects of calorie restriction. *Nature*, (2024). https://doi.org/10.1038/s41586-024-08329-5
15. C. Ma *et al.*, Gut microbiome–mediated bile acid metabolism regulates liver cancer via NKT cells. *Science* **360**, eaan5931 (2018).
16. T. Fu *et al.*, FXR Regulates Intestinal Cancer Stem Cell Proliferation. *Cell* **176**, 1098-1112 e1018 (2019).
17. J. Cong *et al.*, Bile acids modified by the intestinal microbiota promote colorectal cancer growth by suppressing CD8+ T cell effector functions. *Immunity* **57**, 876-889.e811 (2024).
18. S. K. Varanasi *et al.*, Bile acid synthesis impedes tumor-specific T cell responses during liver cancer. *Science* **387**, 192-201 (2025).
19. M. Makishima *et al.*, Identification of a nuclear receptor for bile acids. *Science* **284**, 1362-1365 (1999).
20. D. J. Parks *et al.*, Bile acids: natural ligands for an orphan nuclear receptor. *Science* **284**, 1365-1368 (1999).
21. Y. Kawamata *et al.*, A G Protein-coupled Receptor Responsive to Bile Acids *. *Journal of Biological Chemistry* **278**, 9435-9440 (2003).
22. S. Hang *et al.*, Bile acid metabolites control TH17 and Treg cell differentiation. *Nature* **576**, 143-148 (2019).
23. C. Campbell *et al.*, Bacterial metabolism of bile acids promotes generation of peripheral regulatory T cells. *Nature* **581**, 475-479 (2020).
24. X. Song *et al.*, Microbial bile acid metabolites modulate gut RORgamma(+) regulatory T cell homeostasis. *Nature* **577**, 410-415 (2020).
25. W. Li *et al.*, A bacterial bile acid metabolite modulates Treg activity through the nuclear hormone receptor NR4A1. *Cell Host & Microbe* **29**, 1366-1377.e1369 (2021).
26. D. Paik *et al.*, Human gut bacteria produce TH17-modulating bile acid metabolites. *Nature* **603**, 907-912 (2022).
27. Q. Qu *et al.*, Lithocholic acid binds TULP3 to activate sirtuins and AMPK to slow down ageing. *Nature*, (2024). https://doi.org/10.1038/s41586-024-08348-2
28. E. R. Forster, X. Yang, A. K. Tai, H. C. Hang, A. Shen, Identification of a Bile Acid-Binding Transcription Factor in Clostridioides difficile Using Chemical Proteomics. *ACS Chemical Biology* **17**, 3086-3099 (2022).
29. B. Liu *et al.*, Chemoproteomic Profiling Reveals the Mechanism of Bile Acid Tolerance in Bacteria. *ACS Chemical Biology* **17**, 2461-2470 (2022).
30. X. Yang, X. Zhao, V. Chen, H. C. Hang, Chemical proteomic analysis of bile acid-protein targets in Enterococcus faecium. *RSC Chemical Biology* **3**, 1397-1402 (2022).
31. X. Yang, K. R. Stein, H. C. Hang, Anti-infective bile acids bind and inactivate a Salmonella virulence regulator. *Nature Chemical Biology* **19**, 91-100 (2023).
32. S. Zhuang, Q. Li, L. Cai, C. Wang, X. Lei, Chemoproteomic Profiling of Bile Acid Interacting Proteins. *ACS Cent Sci* **3**, 501-509 (2017).
33. S. Y. Park, S. B. Kim, J. Wan, F. Felice, K. H. Yi, Lipolytic agents for submental fat reduction: Review. *Skin Research and Technology* **30**, e13601 (2024).

34. H. Ishikawa, G. N. Barber, STING is an endoplasmic reticulum adaptor that facilitates innate immune signalling. *Nature* **455**, 674-678 (2008).
35. D. L. Burdette *et al.*, STING is a direct innate immune sensor of cyclic di-GMP. *Nature* **478**, 515-518 (2011).
36. G. N. Barber, STING: infection, inflammation and cancer. *Nature Reviews Immunology* **15**, 760-770 (2015).
37. C. Zhang *et al.*, Structural basis of STING binding with and phosphorylation by TBK1. *Nature* **567**, 394-398 (2019).
38. S. Yum, M. Li, Y. Fang, Z. J. Chen, TBK1 recruitment to STING activates both IRF3 and NF-κB that mediate immune defense against tumors and viral infections. *Proc Natl Acad Sci U S A* **118**, e2100225118 (2021).
39. F. Humphries *et al.*, A diamidobenzimidazole STING agonist protects against SARS-CoV-2 infection. *Science Immunology* **6**, eabi9002 (2021).
40. M. H. Li *et al.*, Pharmacological activation of STING blocks SARS-CoV-2 infection. *Science Immunology* **6**, eabi9007 (2021).
41. B. A. Flood, E. F. Higgs, S. Li, J. J. Luke, T. F. Gajewski, STING pathway agonism as a cancer therapeutic. *Immunological Reviews* **290**, 24-38 (2019).
42. E. N. Chin, A. Sulpizio, L. L. Lairson, Targeting STING to promote antitumor immunity. *Trends in cell biology* **33**, 189-203 (2023).
43. J. M. Ramanjulu *et al.*, Design of amidobenzimidazole STING receptor agonists with systemic activity. *Nature* **564**, 439-443 (2018).
44. E. N. Chin *et al.*, Antitumor activity of a systemic STING-activating non-nucleotide cGAMP mimetic. *Science* **369**, 993-999 (2020).
45. B. S. Pan *et al.*, An orally available non-nucleotide STING agonist with antitumor activity. *Science* **369**, eaba6098 (2020).
46. D. Lu *et al.*, Activation of STING by targeting a pocket in the transmembrane domain. *Nature* **604**, 557-562 (2022).
47. J. Li *et al.*, Activation of human STING by a molecular glue-like compound. *Nature Chemical Biology* **20**, 365-372 (2024).
48. L. Jin *et al.*, Identification and characterization of a loss-of-function human MPYS variant. *Genes & Immunity* **12**, 263-269 (2011).
49. F. Humphries *et al.*, Targeting STING oligomerization with small- molecule inhibitors. *P Natl Acad Sci USA* **120**, e2305420120 (2023).
50. J. Li *et al.*, Activation of human STING by a molecular glue-like compound. *Nat Chem Biol*, **20**, 365-372 (2023).
51. A. Hansel-Harris, A. Tillack, D. Santos-Martins, M. Holcomb, S. Forli, Docking guidance with experimental ligand structural density improves docking pose prediction and virtual screening performance. ChemRxiv (2024) doi:10.26434/chemrxiv-2024-pr56v.
52. L. Corrales *et al.*, Direct Activation of STING in the Tumor Microenvironment Leads to Potent and Systemic Tumor Regression and Immunity. *Cell reports* **11**, 1018-1030 (2015).
53. W. J. Ho, E. M. Jaffee, L. Zheng, The tumour microenvironment in pancreatic cancer — clinical challenges and opportunities. *Nature Reviews Clinical Oncology* **17**, 527-540 (2020).
54. M. Funabashi *et al.*, A metabolic pathway for bile acid dehydroxylation by the gut microbiome. *Nature* **582**, 566-570 (2020).

55. X. Yang, H. C. Hang, Chemical genetic approaches to dissect microbiota mechanisms in health and disease. *Science* **386**, eado8548 (2024).
56. M. F. Gulen *et al.*, cGAS-STING drives ageing-related inflammation and neurodegeneration. *Nature* **620**, 374-380 (2023).
57. Z. Zhang, C. Zhang, Regulation of cGAS–STING signalling and its diversity of cellular outcomes. *Nature Reviews Immunology*, (2025). https://doi.org/10.1038/s41577-024-01112-7

Acknowledgments: We thank the Scripps Research Flow Cytometry and Imaging Cores for technical support.

Funding: This work was supported by National Institutes of Health (NIH) grants 1R01AI182439-01A1 to HCH, CGP, AW, LLL and GM069832 to S.F.

Author contributions:

Conceptualization: XY, XZ, WL, CGP, HCH

Methodology: XY, XZ, WL, AG, AH, AT, CW, Y-ZH, AS, SD, XZ

Investigation: XY, XZ, WL, AG, AH, AT, CW, Y-ZH, AS, SD, XZ

Visualization: XY, XZ, WL, AG, AH, AT, CW, Y-ZH, AS, SD, XZ

Funding acquisition: HCH, CGP, AW, LLL

Project administration: HCH

Supervision: HCH, CGP, AW, LLL, SF

Writing – original draft: XY, XZ, HCH

Writing – review & editing: XY, XZ, WL, AG, AH, SF, LLL, AW, CGP, HCH

Competing interests: LLL has filed and issued patents associated with synthetic STING agonists. All other authors declare that they have no competing interests.

Supplementary Materials

Materials and Methods

Supplementary Text

Figs. S1 to S11

Tables S1

References (*58–69*)

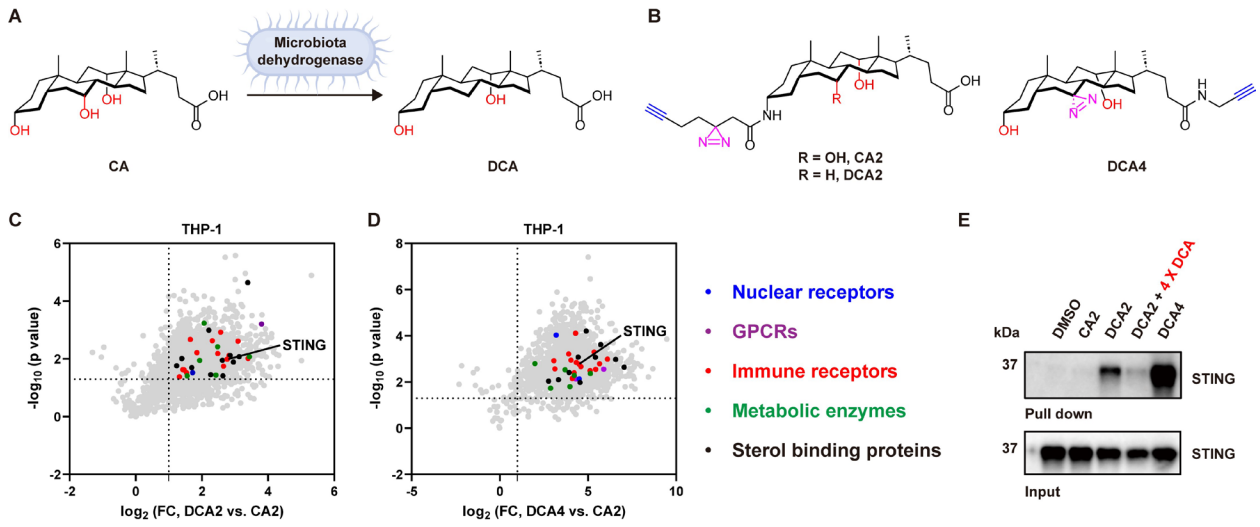

Fig. 1. Proteome-wide mapping of DCA-interacting proteins in mammalian cell reveals DCA-STING interaction. (A) DCA is synthesized from CA by gut microbiota dehydrogenase. (B) Chemical structure of bile acid photoaffinity probes. (C, D) DCA2 (25 μM) and DCA4 (25 μM) bile acid photoaffinity reporters enrich more proteins compared to CA2 in THP-1 cells. STING is one of proteins that are selectively enriched by DCA photoaffinity reporters. Other DCA-enriched proteins are highlighted by different colors. (E) Validation of bile acid-STING interaction in THP-1 by reverse western blot. THP-1 cells were treated with bile acid photoaffinity reporters (25 μM) with or without excess of DCA for 0.5 h, followed by 365-nm light irradiation. The labeled proteins were reacted with az-biotin and enriched with streptavidin beads ('pulldown'). Equal loading was validated by immunoblotting of input samples before enrichment ('input').

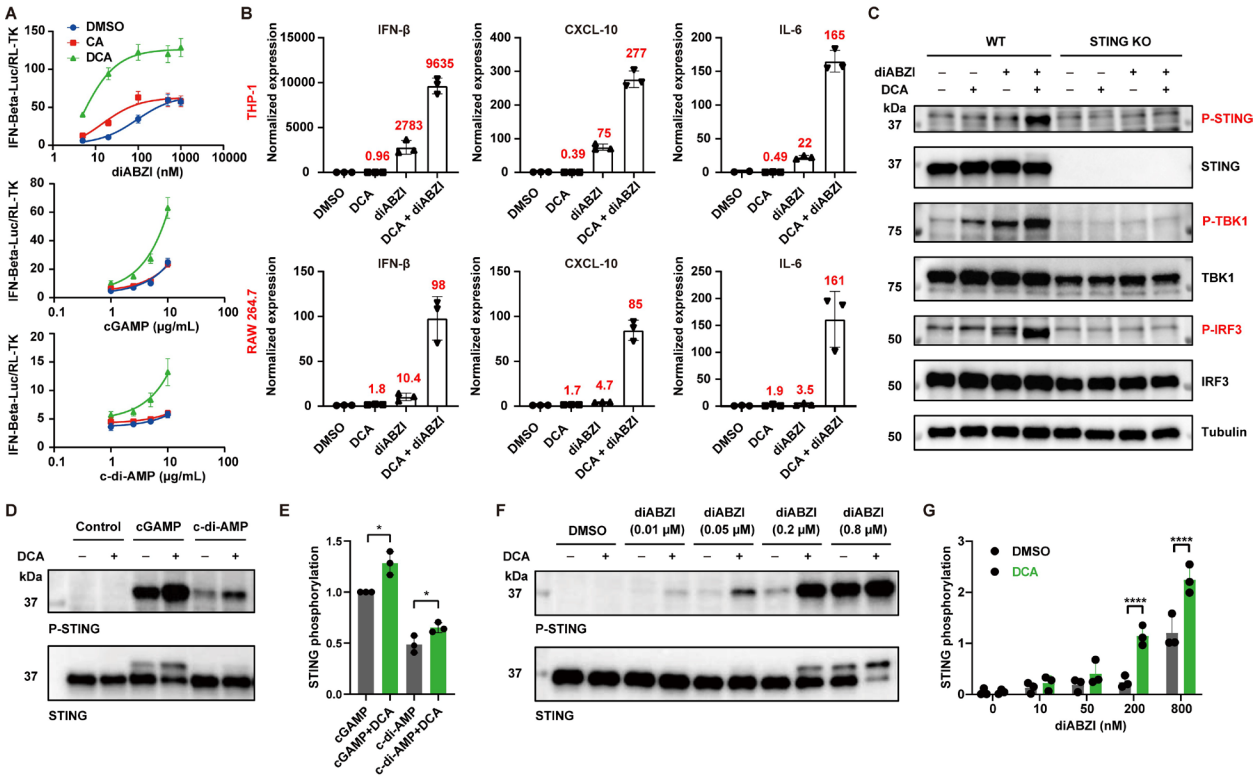

Fig. 2. Bile acids promote STING activation ex vivo. (A) HEK293T transfected with pMSCV-hygro-STING, IFN-Beta_pGL3 (a luciferase reporter plasmid under control of the IFN-β promoter) and pRL-TK control plasmid were treated with different doses of STING agonists (diABZI, cGAMP, c-di-AMP) in presence or absence of DCA and CA (50 μM). (B) qRT-PCR analysis of INF-β, CXCL-10, IL-6 in THP-1 and RAW264.7 cells treated with diABZI (50 nM for THP-1, 200 nM for RAW264.7) and DCA (50 μM) alone or together for 4 hours. (C) Western blot analysis of cell lysates from THP-1 cells (WT and STING KO) treated with diABZI (50 nM) and DCA (50 μM) alone or together for 4 hours. (D) Western blot analysis of cell lysates from Human PBMCs treated with STING agonists (cGAMP (5 μg/mL), c-di-AMP (5 μg/mL), transfected with lipo2000 (1 μg/μL)) and DCA (50 μM) alone or together for 1 hours. (F) Western blot analysis of cell lysates from Human PBMCs treated with different concentration of diABZI with or without DCA (50 μM) for 2 hours. (E, G) Quantification of phosphorylated STING by grayscale analysis (p-STING/STING). *P < 0.05, ****P < 0.0001.

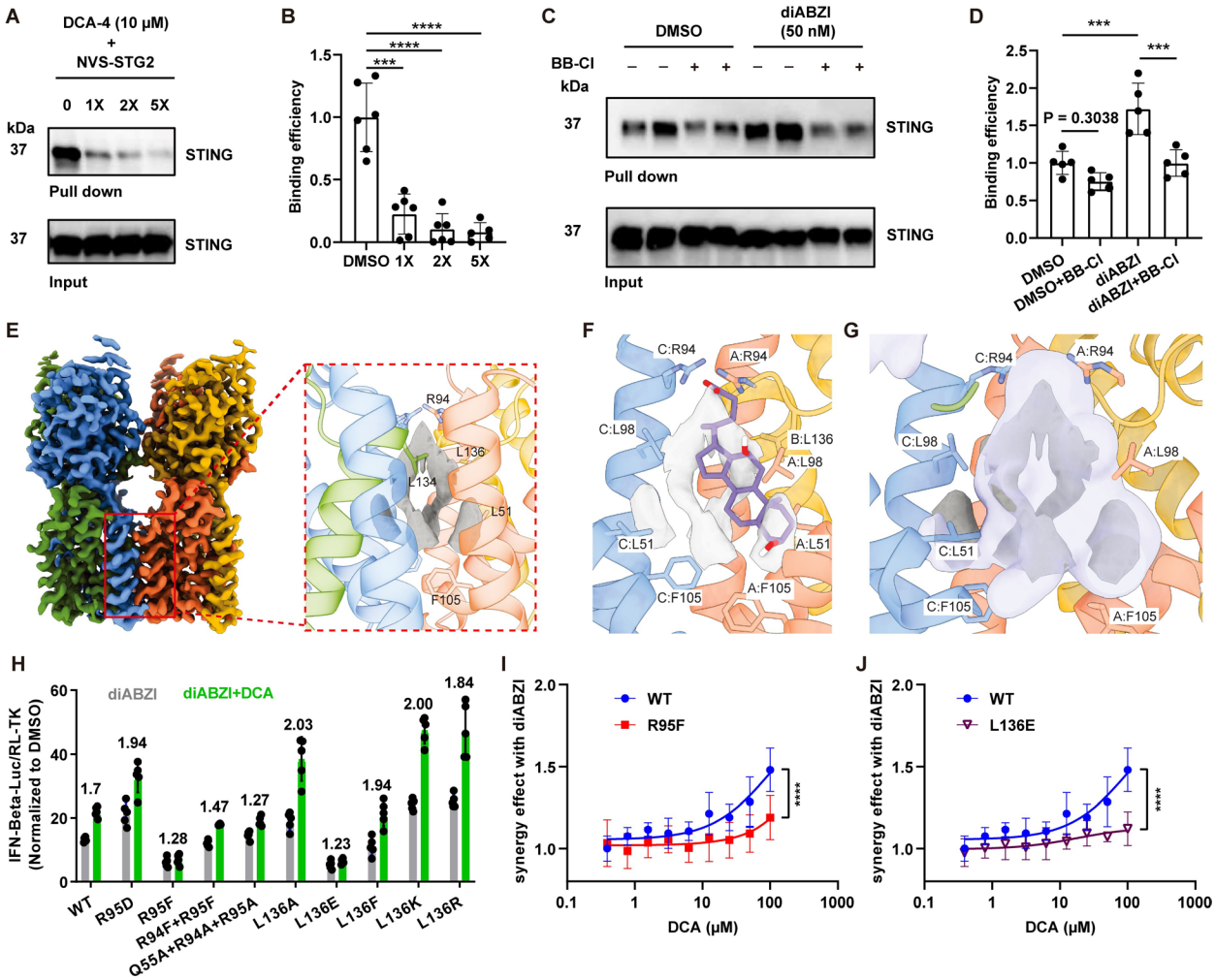

Fig. 3. Bile acids target at STING dimer-dimer interface. (A) HEK293T transfected with pMSCV-hygro-STING were treated with DCA-4 (10 μM) in presence of different concentrations of NVS-STG2 for 30 mins at 37 ºC, followed by 365-nm light irradiation. The labeled proteins in cell lysis were reacted with az-biotin and enriched with streptavidin beads ('pulldown'). Equal loading was validated by immunoblotting of input samples before enrichment ('input'). (B) Quantification of binding efficiency in A by grayscale analysis (pull down/input). (C) THP-1 cells were pretreated with diABZI (50 nM) in presence or absence of BB-Cl (10 μM) for 1 hour. Cells were then treated with DCA-4 (25 μM) for another 0.5 hour, followed by 365-nm light irradiation. The labeled proteins in cell lysis were reacted with az-biotin and enriched with streptavidin beads ('pulldown'). Equal loading was validated by immunoblotting of input samples before enrichment ('input'). (D) Quantification of DCA-4 STING binding efficiency in C by grayscale analysis (pull down/input). (E) High-resolution cryo-EM map of the two STING dimer with highlight of dimer-dimer interface molecular density. (F) Docked model of DCA in STING tetramer. Docking guided by C2-symmetric density, shown in gray. (G) Illustration of docking density cloud (outer violet surface), representing Boltzmann-weighted map of ligand states sampled during docking simulation. All experimental density lobes on one side of the binding pocket were sampled during the simulation, but less so on the opposite side of the pocket. (H-J) HEK293T transfected with pMSCV-hygro-STING (WT and mutations), IFN-Beta_pGL3 and pRL-TK control plasmid were treated with diABZI (20 nM) in presence or absence of DCA. *P < 0.05, **P < 0.01, ***P < 0.001, ****P < 0.0001.

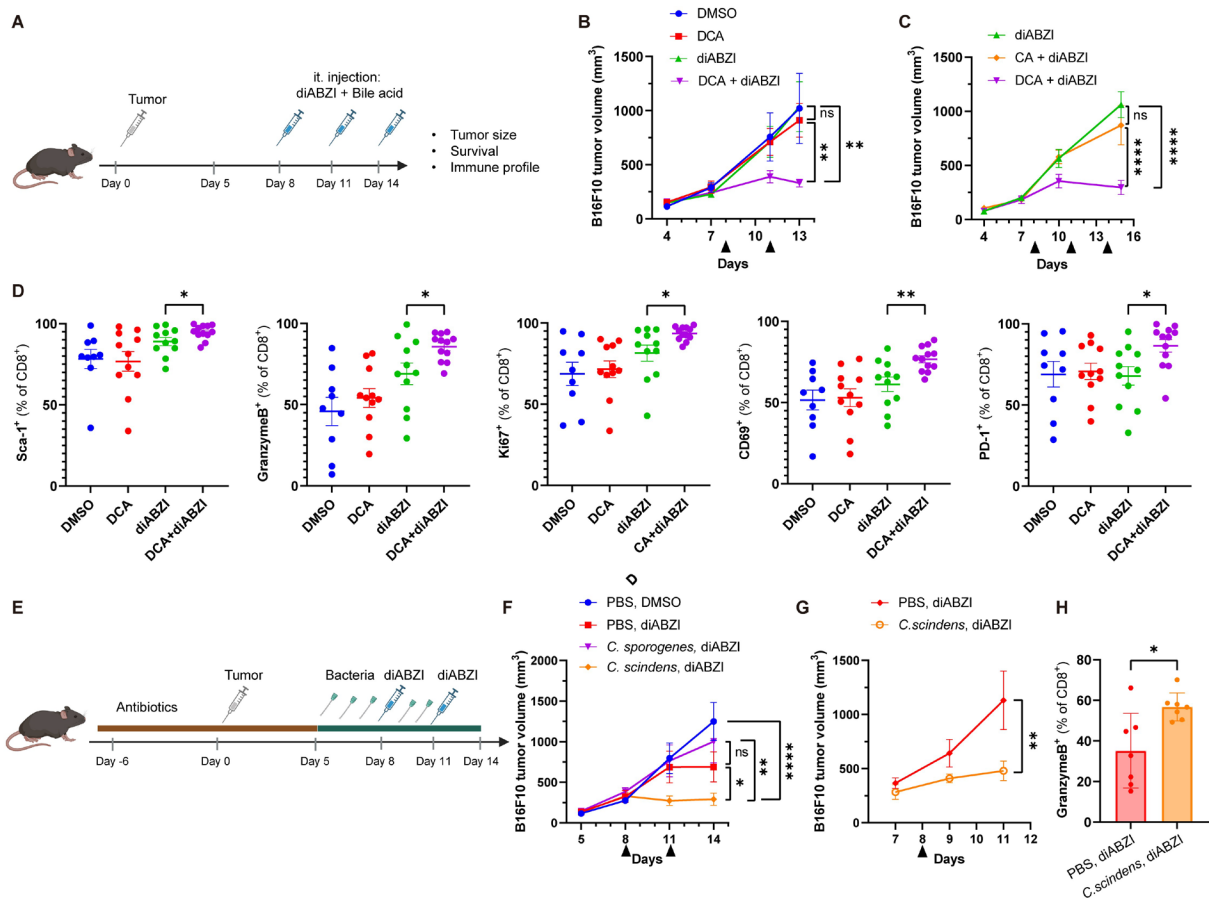

Fig. 4. Bile acid modulation of STING activity *in vivo*. (A) Schematic of *in vivo* tumor model. SPF mice were subcutaneously implanted with tumor cells, and tumor volume measurements started when tumors reached ~50-100 mm^3 (day 4). Mice were treated with diABZI and Bile acids by intratumoral injection every two days started when tumor reached to ~250 mm^3 (day 8). (B) B16-F10 melanoma tumor growth in SPF mice that were it. injected with vehicle (DMSO), bile acids DCA, diABZI or the combination (DCA+ diABZI). (C) B16-F10 melanoma tumor growth in SPF mice that were it. injected with diZBZI alone or together with CA or DCA. (D) Quantification of tumor infiltrating $CD8^+$ T cells from B16-F10 tumors in mice treated with DMSO, DCA, diABZI or the combination. Tumor were harvested 2 days after one dose of it. injection. (E) Schematic illustrating the role of DCA-producing microbiota in modulating STING-mediated antitumor activity. SPF mice were treated with Abx before and after tumor injection to deplete the gut microbiota. Abx treatment was discontinued three days prior to diABZI injection (Day 5) to allow microbiota recolonization. During this period, mice were administered bacteria daily via oral gavage. (F) B16-F10 melanoma tumor growth in Abx-treated mice that were oral garaged with PBS, *C. sporogenes* or *C. scindens* and it. injected with DMSO or diABZI at Day8 and Day11. (G) B16-F10 melanoma tumor growth in SPF mice without Abx treatment that were oral gavage with PBS or *C. scindens* and it. injected with diABZI. (H) Quantification of tumor infiltrating $GranzymeB^+$ $CD8^+$ T cells from (G). n = 7 per group. Data for (B), (C), (F) and (G) represent mean ± SEM and were analyzed using a mixed effects model with Tukey's multiple comparisons post hoc test. n=8 mice per group. Arrowhead indicates the day for it. injection. Data for (D) and (H) represent mean ± SEM and were analyzed by the unpaired t test. Data for (D) were pooled from two independent experiments. n=9-12 per group. Each symbol represents one mouse. *P < 0.05, **P < 0.01, ***P < 0.001, ****P < 0.0001; ns, not significant.